A&A 454, 833–838 (2006)
DOI: 10.1051/0004-6361:20042498

Astronomy & Astrophysics

Spectrometric composition of nearby K dwarfs⋆

E. Kotoneva[1,2], J. R. Shi[1], G. Zhao[1], and Y. J. Liu[1]

[1] National Astronomical Observatories, Chinese Academy of Sciences, Beijing 100012, PR China
e-mail: gzhao@bao.ac.cn
[2] Turku University, Tuorla Observatory, Väisäläntie 20, 21500 Piikkiö, Finland

Received 7 December 2004 / Accepted 2 August 2005

ABSTRACT

We have obtained relatively high resolution spectra of Northern hemisphere K dwarfs. This is the first spectrometric project dedicated only to K dwarfs. Earlier studies have concentrated on more massive F and G dwarfs. However, these stars have already undergone evolutionary effects, unlike K dwarfs, which offer more accurate information about the evolution of the Solar neighbourhood. We have determined the LTE abundances of 14 elements for 42 stars with initial metallicity range covered by $-1.52 < [Fe/H] < 0.48$. We confirm the discrepancy in the abundances derived from neutral and ionized lines. The solution to this problem cannot just be the modification of initial physical parameters, but requires fundamental changes in the modeling of K dwarfs.

Key words. stars: abundances – stars: low mass, brown dwarfs – Galaxy: solar neighbourhood

1. Introduction

Many spectroscopic studies of the F and G dwarfs have been performed in recent years (e.g. Edvarsson et al. 1993; Chen et al. 2000). These stars, however, are not the most ideal tool to study our Galaxy from the point of view of galactic chemical evolution (GCE) since they already suffer from the effects of stellar evolution, i.e. some of them may have already left the main sequence. Thus studies of GCE should use low mass K dwarfs instead. These stars have low mass and their lifetime is very long, even longer than the age of the Galaxy itself, a sample of K dwarfs can more reliably trace the evolution of our Galaxy.

We have obtained relatively high resolution spectra with a signal to noise ratio from 80 upto 280 for 42 nearby K dwarfs with absolute magnitude range covered by $5.5 < M_V < 7.3$. This is the first spectrometric study dedicated to K dwarfs. Care has been taken in obtaining the physical parameters i.e. effective temperature $T_{\rm eff}$, surface gravity log g and microturbulent velocity ξ. A wide spectral coverage offers us an opportunity to study a large number of different elements simultaneously.

Due to lack of the spectroscopic data of K dwarfs, the general trends of this work have been compared with a previous study concentrating on F and G dwarfs (Chen et al. 2000, hereafter Chen00). Previous comparisons between the metallicities of G and K stars have shown (e.g. Kotoneva et al. 2002) that the general behaviour of these two star types are very alike. This indicates that despite the different lifetime these stars share similar evolutional histories. Compared to Chen00, this study has an additional element, scandium. We also compared our results to the resent study by Prieto et al. (2004). These comparisons concentrate on the differences in the metallicities derived from neutral and ionized lines. The differences in our work are as large as 0.31 dex, and it does not seem likely to be resolved by fixing the initial physical parameters of the stars, because the problem only arises for stars with either very high or low effective temperatures, and it also affects both surface gravity and microturbulent velocity.

This paper is organized as follows. In Sect. 2 the data and observations are described. The physical parameters are discussed in Sect. 3 and atomic line data is presented in Sect. 4. In Sect. 5 the LTE abundances are presented and in Sect. 6 we show the final results. The conclusions are drawn in Sect. 7.

2. Data and observations

2.1. The selection of stars

Our sample of K dwarfs was drawn from the ESA Hipparcos catalog (ESA, 1997). We take K dwarfs to be stars of absolute magnitude M_V in the range $5.5 < M_V < 7.3$. The upper magnitude limit at $M_V = 5.5$ is chosen to avoid the effects of stellar evolution. Examination of theoretical isochrones (see e.g. Jimenez et al. 1998) indicates that the effects of stellar evolution on luminosity at $M_V = 5.5$ during the disc lifetime amount to at most 0.1 mag, and are typically much smaller. The effects of stellar evolution in constructing the sample are thus small, and negligible compared to the main source of error (which is Poisson sampling statistics). The limit at $M_V = 5.5$ corresponds to a spectral type of about G8. The lower absolute magnitude limit at $M_V = 7.3$ is the magnitude of the reddest K dwarfs for which our photometric metallicity indicators can currently be calibrated via spectroscopic observations (Flynn & Morell 1997). The limit at $M_V = 7.3$ corresponds a spectral type of about K 5, the stars were initially selected from the "survey" part of the Hipparcos catalog, which is complete to an apparent visual magnitude given by $V < 7.3 + 1.1 \sin|b|$, where b is the Galactic latitude (the apparent visual magnitude limit was made dependent on b in order to avoid observing excessive numbers of stars in the Galactic plane). All the known multiple systems were removed on the basis of the Hipparcos catalogue flag, and all suspected binaries were also removed. The original sample is described in detail in Kotoneva et al. (2002).

⋆ Tables 1–4 and Figs. 12–14 are only available in electronic form at http://www.edpsciences.org

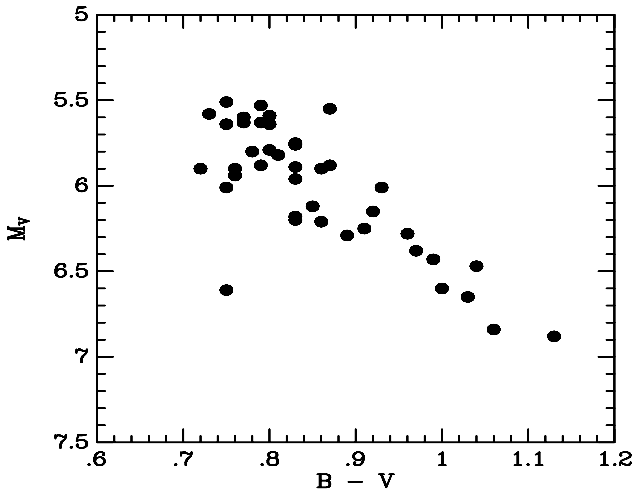

Fig. 1. The colour−magnitude diagram for the stars in this paper.

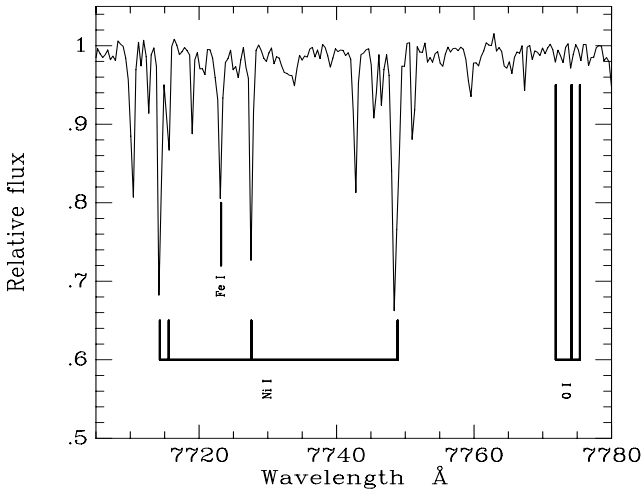

Fig. 2. The example of the spectrum of HD 84035 zoomed to the wavelength range between 7700 and 7780 Å.

We observed high resolution spectra for as many Northern hemisphere stars as possible. The primordial metallicities $[Fe/H]_{KF}$, i.e. metallicities based on the study by Kotoneva et al. (2002), are calculated on the basis of stars' magnitude and distance from the reference isochrone described in that paper, the initial metallicity for the 42 stars that are observed in the present study is in the range of $-1.52 \leq [Fe/H] \leq 0.48$. In Fig. 1 the colour magnitude diagram for the program stars is shown.

2.2. Observations and data reduction

The observations were taken with the Coude Échelle Spectrograph at the 2.16 m telescope of the National Astronomical Observatories (Xinglong, China) in two runs during 2003. The first observations were taken between 11th and 18th of March and the second run between 9th and 12th of September. The detector was a Tek CCD (1024×1024 pixels with 24×24 μm^2). The spectra cover the wavelength range 5600−8800 Å.

The data were reduced using the standard MIDAS routines for order identification, background subtraction, flat field correction, order extraction and wavelength calibration. Before determining the equivalent widths the spectra were normalized to the continuum function and corrected for the radial velocity shift. The example of a spectrum with some identified lines is shown in Fig. 2.

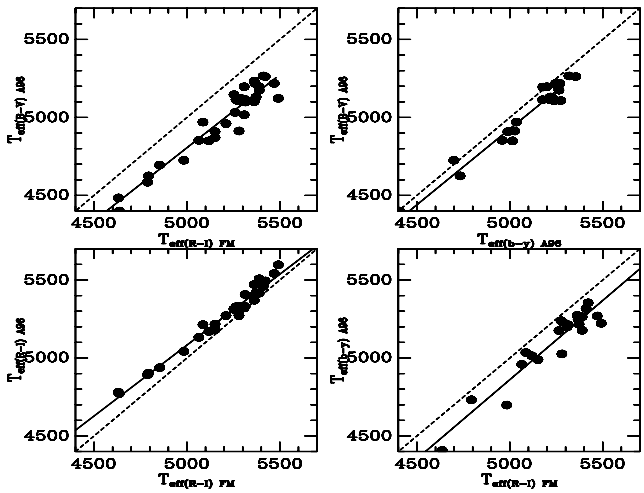

Fig. 3. *Lower left panel*: comparison between the temperatures based on $R-I$ colours (FM97 and Alonso). The agreement is good, however some drift is seen at low temperatures. The lower right panel and the upper left panels show the comparisons between the colours after the FM97 indicator and temperatures based on Strömgren colours and $B-V$. The $R-I$ based colours imply systematically higher temperatures. Finally the upper right panel shows the comparison between the Strömgren and $B-V$ colours; as expected they agree well. The solid lines are the least square fits.

3. Physical parameters

3.1. Effective temperature

There are many different effective temperature indicators in the literature. We use the calibration formula for the $R-I$, $B-V$ and $b-y/c_1$ colours from Alonso et al. (1996) and for the $R-I$ colour from Flynn & Morell (1997, hereafter FM97). These were compared again each other to find the most reliable temperature indicator. The comparison is shown in Fig. 3.

On the basis of these comparisons the initial effective temperatures were calculated using three different methods: firstly, since the errors in the $R-I$ colour are very small, usually less than 0.01 mag (Kotoneva et al. 2002), and it is also known to be independent of the temperature (FM97), it was chosen as the main $T_{\rm eff}$ indicator. For those 33 stars that have $R-I$ colours available, the effective temperatures were calculated according to the method given by Flynn & Morell (1997). Secondly, for the stars that did not have a $R-I$ colour index, the relation between the effective temperature, metallicity and the Strömgren $b-y$ and c_1 colours were taken from Alonso et al. (1996). For the rest of eight stars, with neither $R-I$ nor Strömgren colours available, the $B-V$ colour index was used to define the effective temperature. The errors of the effective temperature for all systems are about 50−70 K.

The effects of different effective temperatures were studied. The change of the $T_{\rm eff}$ has different effects on metallicities derived from $[Fe_I/H]$ and $[Fe_{II}/H]$. For example if the effective temperature increases by 100 K, the mean metallicity $[Fe/H]_I$ decreases by 0.06 dex, while the mean metallicity $[Fe/H]_{II}$ increases by 0.07 dex. The effects on the final metallicities were

quite small, since the temperatures differ by less than 150 K. It was also noticed that the stars with especially low temperatures, $T_{\rm eff} < 5000$ K, gave inaccurate metallicities than the stars with intermediate temperatures.

3.2. Metallicity

The initial metallicities $[{\rm Fe/H}]_{KF}$ for the stars were taken from Kotoneva et al. (2002), in which they were calculated on the basis of K dwarf luminosity M_V, colour index $B-V$ and the star's displacement from a fiducial isochrone. The fiducial isochrones come from Jimenez et al. (1998). We found that metallicities using this technique are greatly superior to photometrically derived metallicities. The typical error in the metallicities was found to be about 0.1 dex.

3.3. Surface gravity

Surface gravities were determined from the Hipparcos parallaxes by using following equation:

$$\log\, g \;=\; \log\frac{M}{M_\odot} + 4\times\log\frac{T_{\rm eff}}{T_{\rm eff\odot}} \qquad (1)$$
$$+0.4\times(M_{\rm bol} - M_{\rm bol\odot}) + \log\, g_\odot,$$

where $T_{\rm eff\odot} = 5780$ K, $M_{\rm bol\odot} = 4.83$ and $\log\, g_\odot = 4.44$.

The bolometric correction were defined using the BC grids of Alonso et al. (1995).

The mass of the stars is calculated based on the latest isochrones by Jimenez (private communication). Three metallicity limits were used, [Fe/H] = −0.50, 0.00 and 0.30, and the age was set to be 12 Gyr. The effect of age on the mass was studied and it was shown that the mass difference between the stars of age 1 Gyr and 14 Gyr was less than 0.1 $M_\odot$, which means that the change in the surface gravity is less than 0.05 dex, at maximum less than 10%, i.e. four stars, would have age around 1 Gyr, so the uncertainties in the log g are always small.

3.4. Microturbulence

The microturbulences were calculated using the equations by Nissen (1981). We tested the microturbulences by investigating the slope of $[{\rm Fe_I/H}]$ vs. EW. It is showed that the abundances (log(Fe I)) were independent of EW (see Fig. 4). This is a reliable way to test the microturbulent velocity since there are around 50 Fe I lines for most of the stars.

The stellar atmospheric parameters for the program stars are shown in Table 1. The columns are HD number, Hipparcos input number, effective temperature $T_{\rm eff}$, surface gravity log g, initial metallicity $[{\rm Fe/H}]_{\rm KF}$, microturbulent velocity ξ, bolometric correction $B.C.$ and mass.

3.5. Comparison with the NStar study

Recently, Gray et al. (2003) published the first part of the ongoing Nearby Stars-project. Among their dataset there were 14 stars common to this study. We compared their physical parameters, log g, $T_{\rm eff}$ and [Fe/H] against our values and we also calculated the spectroscopic metallicities for these stars using their parameters. The surface gravity comparison is shown in Fig. 5.

The effective temperatures, $T_{\rm eff}$, were tested with different methods. The comparison of effective temperature is shown in Fig. 6. This plot shows that the temperatures are in quite good agreement with each other except for two stars (HD 114783 and HD 128311). For both stars the effective temperatures were also calculated using Strömgren colour indices and the $B-V$ colour index which both give even lower values than the $R-I$ colour index. It seems that stars with low effective temperatures are more sensitive to the colour indices and also to the errors in the colours. The difference $[{\rm Fe/H}]_{\rm I} - [{\rm Fe/H}]_{\rm II}$ was −0.06 dex for NStar, about 0.30 dex and −0.20 dex for our high and low temperature stars, respectively, so the discrepancy is large whatever values you use.

In Fig. 7 the comparison between this work and the NStar study for the metallicities is shown. Except for four stars with large differences, the agreement is generally good. The spectroscopic metallicities were calculated for these 14 common stars using stellar parameters from Gray et al. (2003) and the results are shown in Table 2.

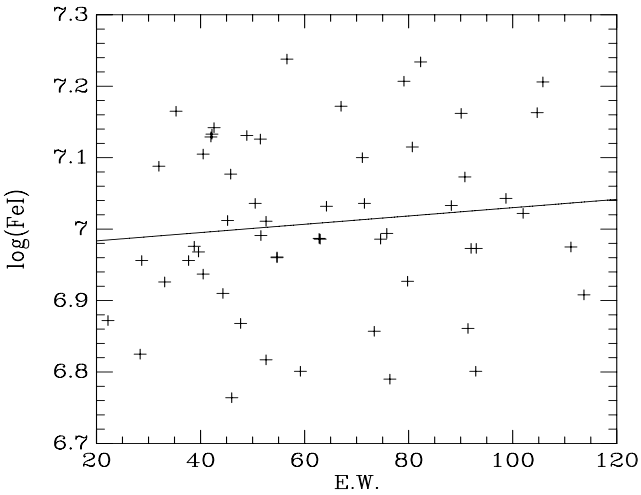

Fig. 4. The log (Fe_I) as a function of equivalent widths EW of HD 24238. The line shown has a slope less than 0.001 dex.

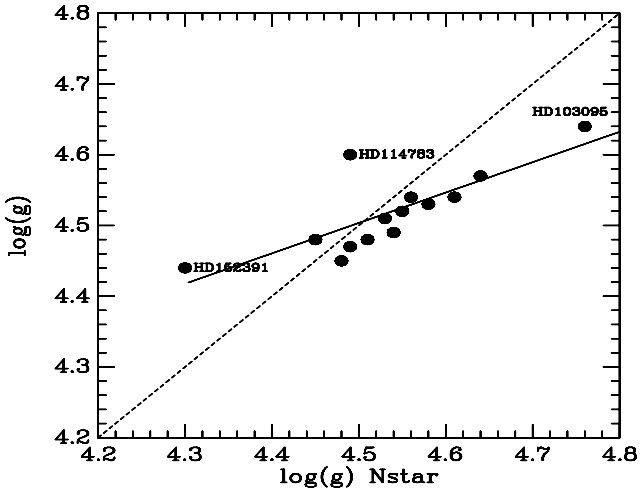

Fig. 5. Comparison of the surface gravity between the NStars and this study. The solid line is the least square fit. As can be been in this figure this study estimates most of the surface gravities to be lower than the NStar work, expect for two stars (HD 114783 and HD 152391) with higher values of log g. There is also one star with lower value (HD 103095). The standard deviation of the least square fit is ≈0.04 dex.

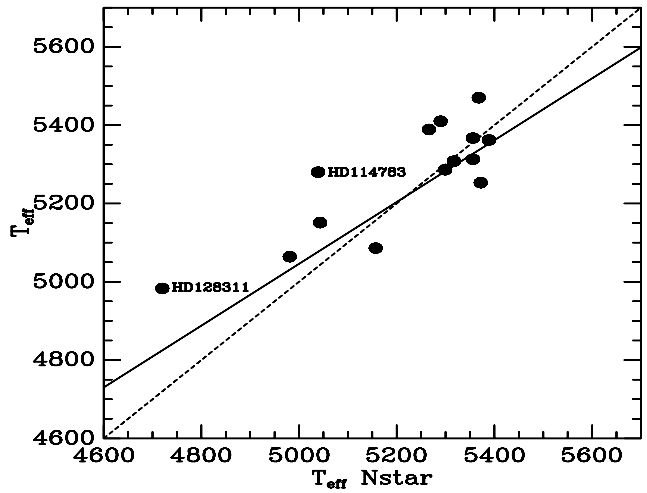

Fig. 6. The comparison of the effective temperatures between this study and the NStar work. The solid line is the least square fit when the errors in both temperatures were taken into account. The standard deviation is 80 K.

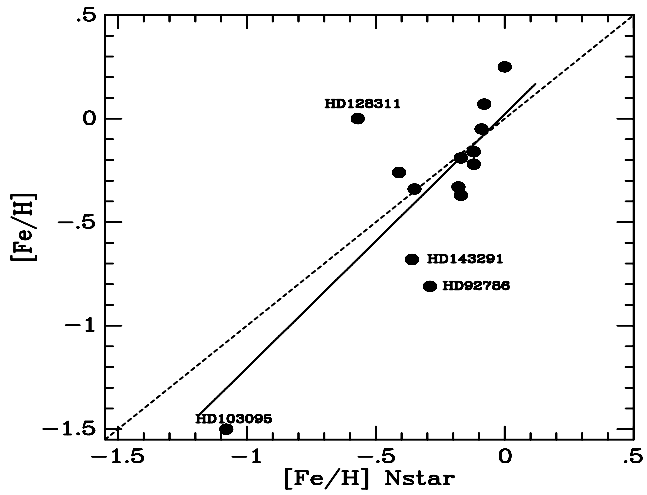

Fig. 7. The comparison between the initial metallicities of this study and the NStar work. The solid line is the least square fit; the standard deviation is 0.24 dex.

4. Atomic line data

4.1. Spectral lines

Most of the lines used in this work are the same as those in Chen00, Tomkin et al. (1997) and Castro et al. (1997). All additional lines were chosen from the NIST database (`http://www.physics.nist.gov/`). Those Fe I lines that have equivalent widths larger than 120 mÅ were not taken into account in calculations. For the rest of the lines the limit was 150 mÅ.

4.2. Oscillator strengths and excitation energies

The oscillator strength $\log gf$ and the excitation energies χ_l are mainly taken from the NIST database (`http://www.physics.nist.gov`). The rest are the same as in Chen00.

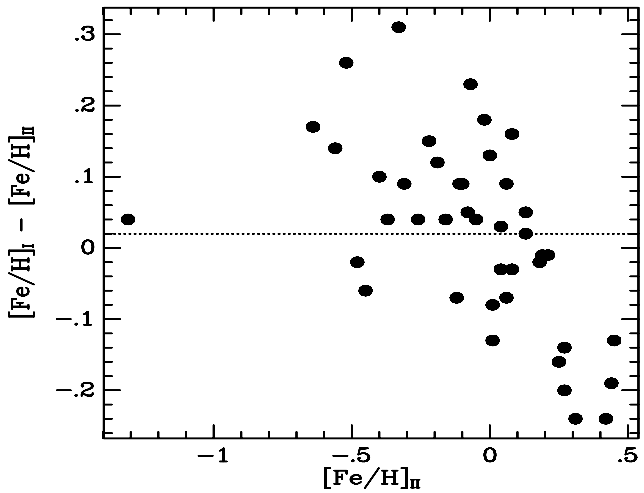

Fig. 8. Differences in the iron abundances derived from $[Fe/H]_I$ and $[Fe/H]_{II}$ lines versus $[Fe/H]_{II}$. The range in differences is quite large, the σ of the plot is 0.13 dex and the mean, shown as a dashed line, is 0.02.

4.3. Empirical enhancement factors and model atmosphere

The choice of damping enhancement factors $f6$ for different elements follows Chen00. The model atmosphere used here was essentially the same as the Atlas 9 by Kurucz (1993). The Solar abundances are taken from Grevesse et al. (1998).

The atomic line data is shown in Table 4.

5. LTE abundances

The abundances were calculated with the analysis program ABONTEST, which was kindly supplied by Magain (Liège, Belgium). The calculations include natural broadening, thermal broadening, van der Waals damping and microturbulent broadening. For most of the stars the following element abundances were calculated: Fe I, Fe II, O I, Na I, Mg I, Al I, Si I, Ca I, Ca II, Sc II, Ti I, V I, Cr I, Ni I, Ba II, K I. The full dataset for the LTE abundances is shown in Table 3.

5.1. Iron abundances

There is a large scatter in the differences between the metallicities $[Fe/H]_I$ and $[Fe/H]_{II}$. In Fig. 8 the difference of the metallicities derived from $[Fe/H]_I$ and $[Fe/H]_{II}$ is shown as a function of $[Fe/H]_{II}$. Most of the stars lie between ±0.20 dex and usually $[Fe/H]_{II}$ tends to give higher metallicities. Also the slopes of effective temperature, surface gravity and $[Fe/H]_{II}$ vs. Δ[Fe/H] are very pronounced (see Fig. 9). In Fig. 10 the same relations are shown against Δ[Ca/H].

When comparing the initial metallicities with new spectroscopic ones, there was found to be a slight increase in new metallicities. The average difference for $[Fe/H]_I$ is 0.14 dex and for $[Fe/H]_{II}$ is 0.12 dex. As seen in Fig. 11 the metallicities are in quite good agreement for $[Fe/H] \geq -0.60$ dex; after this the discrepancy becomes larger.

5.2. Errors of abundance

The effect of the changes in the initial data, i.e. the effective temperature, surface gravity and microturbulent velocities were discussed in Sect. 3. An additional error source might be the equivalent widths, which tend to be more difficult to define for K dwarfs

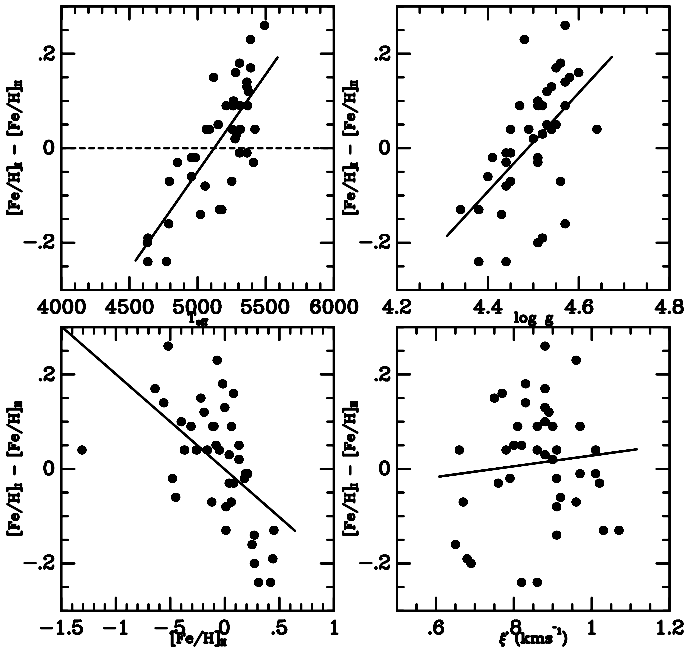

Fig. 9. *The upper left plot* shows the relation between the Δ[Fe/H] and the effective temperature. The differences are very large for both low and high metallicities and the trend is very similar to Prieto et al. (2004). *The upper right plot* shows the relation between the Δ[Fe/H] and surface gravity; the comparison with Prieto et al. (2004) was difficult since they have much broader log g values, but the trend is still very clear. *The lower left plot* shows the same relation between the Δ[Fe/H] and $[Fe/H]_{II}$. *The lower right plot* shows the relation between the Δ[Fe/H] and the microturbulent velocity; again the dependence is clear.

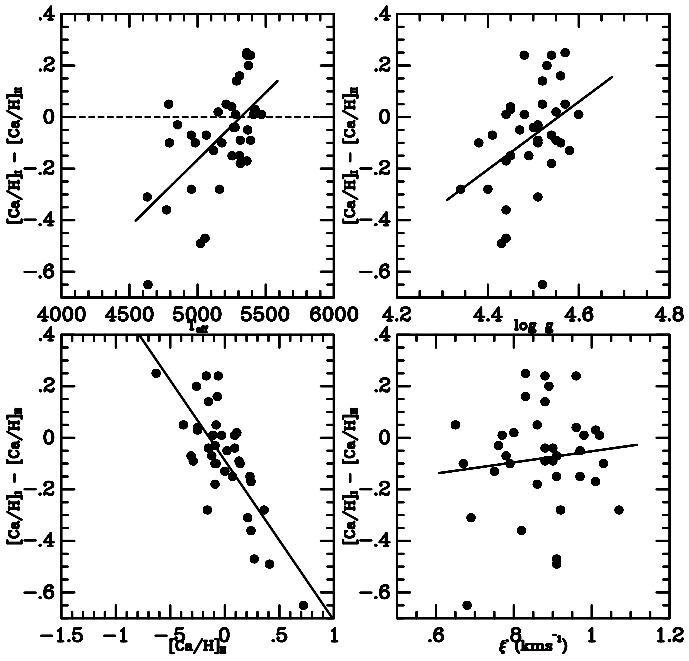

Fig. 10. Same as Fig. 9, but for calcium abundances. The same relations are clearly shown.

than for more massive stars. Some errors on relative abundances can occur because of the differences in the abundances derived from neutral and ionized lines. However, the LTE abundances of the elements, excluding Ca and Fe, should be free of this effect, and thus quite accurate.

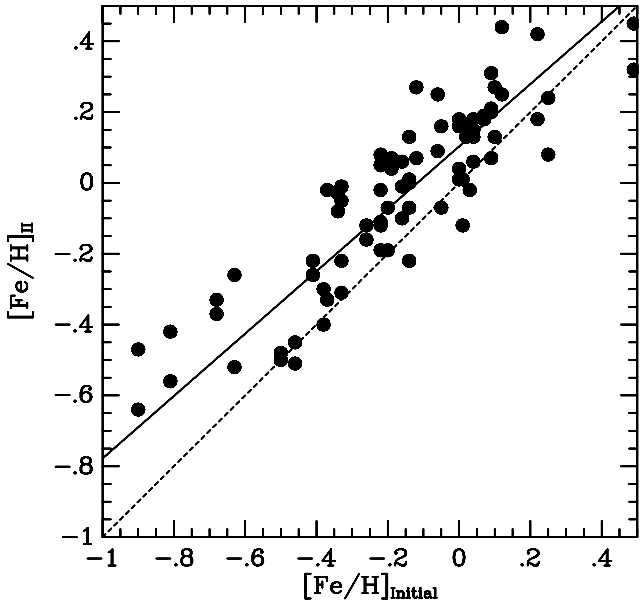

Fig. 11. The newly calculated $[Fe/H]_{II}$ metallicities versus the initial metallicities $[Fe/H]_{KF}$. The solid line is the least square fit. The standard deviation of the fit is 0.12 and the slope of the fit is 0.88.

6. Results

6.1. Relative abundances

In the literature there has been no study of a large sample of K dwarfs available, so the pattern comparisons have been carried out using the Chen00 G dwarf study as a comparison data set. As has been pointed out in earlier studies (e.g. Kotoneva et al. 2002), there is no clear difference between K and G metallicity distributions, which indicates that the trends of rest elements are alike.

We compared the general trends of 14 elements (Fe, O, Na, Mg, Al, Si, K, Ca, Sc, Ti, V, Cr, Ni and Ba). The comparisons are shown in Figs. 12−15.

6.1.1. Oxygen and magnesium

Oxygen is by far the most studied element because it offers information about both galactic and stellar evolution. In this work oxygen shows a slightly large scatter in relative abundances compared to Chen00 and the slope in low metallicities seems to be steeper in this study. HD 103095 shows very high oxygen abundance, which agrees with the known trend of oxygen; [O/Fe] decreases with increasing metallicity. The oxygen abundances seem to start rising again in super-solar metallicities, but more data is needed to confrim this. Magnesium has a steep slope for [Fe/H] > -0.50 dex in our plot; for metallicities lower than this the curve seems to be flat. Because of the small number of stars with low metallicities, we cannot be sure if the flat is real. The magnesium abundances usually keep increasing with decreasing metallicity, as seen in the comparison plot by Chen00.

6.1.2. Silicon, calcium and titanium

For silicon, the scatter is quite small and [Si/Fe] remains nearly flat for all metallicities, except for a few stars, that a slight decrease with increasing metallicity is also seen in Chen00. For calcium the scatter is greater, since the plot shows both $[Ca/Fe]_I$

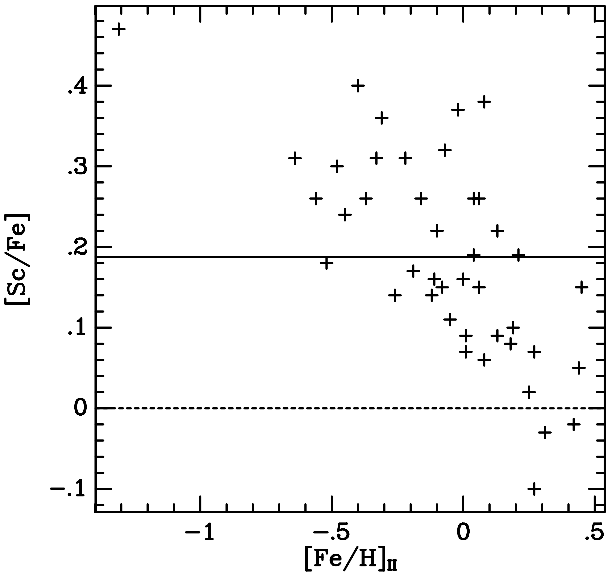

Fig. 15. General trends for scandium.

and $[Ca/Fe]_{II}$. Otherwise, the plot agrees with Chen00, i.e. showing only a slight increase of [Ca/Fe] for lower metallicities. This trend is similar for titanium, although the scatter is quite large.

6.1.3. Sodium and aluminium

[Na/Fe] steadily decreases from [Fe/H] ≈ -0.5 to 0.5 in our plot, whereas in Chen00's plot the values always remain near 0.00. Despite that the scatter is large, the main trend of sodium is flat, although due to the small number of stars the increase of sodium in metal-rich stars cannot be seen. Aluminium has a steep slope and the increasing of [Al/Fe] for higher metallicities cannot be seen, as in Chen00.

6.1.4. Potassium

Potassium has a strong relation with the metallicity; [K/Fe] decreases strongly with increasing metallicity which agrees well with Chen00. The explanation for such a strong trend is that potassium is known to be produced in massive oxygen burning stars.

6.1.5. Vanadium, chromium and nickel

Vanadium, chromium and nickel all agree quite well with Chen00. Despite the large scatter they show only slight changes in their average abundances as a function of metallicity.

6.1.6. Barium

Barium abundances first increase with increasing metallicity and then drop for super-solar metallicities. The trend is more pronounced in our study than in Chen00 and it is also seen in other studies (e.g. Prieto et al. 2004).

6.1.7. Scandium

Prieto et al. (2004) suggest that scandium follow very closely the behavior of silicon and titanium; this agrees well with our study. Scandium remains nearly flat for all metallicities, showing a slight decrease with increasing metallicity. Scandium is known to be produced in massive stars, which can be seen as an overabundance of 0.2 dex at low metallicities; this was also shown in previous studies e.g. Chen (2000).

7. Conclusions

In this work the spectroscopic abundances have been derived for 42 nearby K dwarfs. It is shown that the trends of K dwarfs are generally the same as earlier G dwarfs. This work currently does not take into account non-LTE effects, but the project is still ongoing.

We found that there are some systematic differences of the abundances derived from neutral and ionized lines, especially for the stars with very low or high effective temperatures. Care has been taking in defining the physical parameters, so it is unlikely that only they could explain the problem since e.g. the change in the effective temperature should then be as large as 250 K for our stars. This is far higher than the mean difference or standard deviation of the temperatures calculated using different temperature indicators compared in this work and that all gave similar results for our program stars. Neither can the change in surface gravity explain this difference. This problem has been reported e.g. by Feltzing and Gustafsson (1998), Schuler et al. (2003) and Prieto et al. (2004). Prieto et al. suggested that the explanation could be connected to the modeling, i.e. LTE, surface convection or incomplete opacities.

We agree with Prieto et al. that there are problems in the classical abundance analysis and more precise theoretical models are needed before we can rely on results of K dwarf stars.

Acknowledgements. This work has been financially supported by the Vilho, Yrjö and Kalle Väisälä Foundation, the Magnus Ehrnrooth Foundation, the Academy of Finland and the National Natural Science Foundation of China under grants Nos. 1043010 and 10521001. EK thanks the National Astronomical Observatories of China for its hospitality during her visits.

References

Alonso, A., Arribas, S., & Martinez-Roger, C. 1995, A&A, 297, 197
Alonso, A., Arribas, S., & Martinez-Roger, C. 1996, A&A, 313, 873
Castro, S., Rich, R. M., Grenon, M., Barbuy, B., & McCarthy, J. K. 1997, AJ, 114, 376
Chen, Y. Q. 2000, Ph.D. Thesis, The Department of Astronomy, Beijing Normal University
Chen, Y. Q., Nissen, P. E., Zhao, G., Zhang, H. W., & Benoni, T. 2000, A&AS, 141, 491
Edvardsson, B., Andersson, J., Gustafsson, B., et al. 1993, A&A, 275, 101
ESA 1997, The Hipparcos and Tycho Catalogues, ESA, SP-1200
Feltzing, S., & Gustafsson, B. 1998, A&AS, 129, 237
Flynn, C., & Morell, O. 1997, MNRAS, 286, 617
Gray, R. O., Corbally, C. J., Garrison, R. F., McFadden, M. T., & Robinson, P. E. 2003, AJ, 126, 2048
Grevesse, N., & Sauval, A. J. 1998, SSRv, 85, 161
Jimenez, R., Flynn, C., & Kotoneva, E. 1998, MNRAS, 299, 515
Kotoneva, E., Flynn, C., Chiappini, C., & Matteucci, F. 2002, MNRAS, 336, 879
Nissen, P. E. 1981, A&A, 97, 145
Kurucz, R. L. 1993, CD-ROM No. 13, 18, Smithsonian Astrophysical Observatory
Prieto, C. A., Barklem, P. S., Lambert, D. L., & Cunha, K. 2004, A&A, in press
Schuler, S. C., King, J. R., Fischer, D. A., Soderblom, D. R., & Jones, B. F. 2003, AJ, 125, 2085
Tomkin, J., Edvardsson, B., Lambert, D. L., & Gustafsson, B. 1997, A&A, 327, 587

Online Material

Table 1. The stellar atmospheric parameters for the program stars.

HD	HIP	$T_{\rm eff}$ [K]	log g	[Fe/H]$_{\rm KF}$	ξ [km^{-1}]	*B.C.*	Mass [$M_\odot$]	Note
21742	16581	5161.	4.34	0.49	1.07	−0.32	0.88	c
24238	18324	4954.	4.41	−0.50	0.91	−0.44	0.74	c
29883	21988	5118.	4.58	−0.14	0.75	−0.30	0.80	a
32237	23431	5388.	4.55	−0.90	0.88	−0.24	0.78	a
37008	26505	4955.	4.41	−0.46	0.92	−0.44	0.74	c
41593	28954	5363.	4.54	−0.14	0.88	−0.22	0.84	a
51866	33852	4852.	4.51	0.00	0.75	−0.40	0.78	a
59747	36704	5152.	4.53	−0.34	0.82	−0.31	0.74	a
60272	37061	5371.	4.53	−0.20	0.89	−0.22	0.84	a
72760	42074	5389.	4.48	−0.05	0.96	−0.22	0.86	a
76218	43852	5367.	4.47	−0.16	0.97	−0.22	0.86	a
82443	46843	5255.	4.49	−0.33	0.91	−0.20	0.80	a
84035	47690	4638.	4.52	0.12	0.67	−0.57	0.74	a
87883	49699	4772.	4.44	0.09	0.81	−0.36	0.80	c
89813	50782	5470.	4.48	−0.37	0.98	−0.25	0.83	a
92786	52470	5362.	4.57	−0.81	0.83	−0.23	0.77	a
94765	53486	5149.	4.55	0.04	0.80	−0.31	0.81	a
97658	54906	5211.	4.52	−0.33	0.86	−0.33	0.75	a
98281	55210	5420.	4.45	−0.41	1.01	−0.24	0.84	a
102195	57370	5312.	4.51	0.04	0.90	−0.20	0.85	a
103095	57939	5083.	4.64	−1.50	0.66	−0.30	0.67	a
103847	58314	5276.	4.50	0.02	0.90	−0.19	0.85	a
105631	59280	5362.	4.44	0.09	1.00	−0.21	0.87	a
108984	61099	5309.	4.56	0.03	0.83	−0.20	0.83	a
114783	64457	5280.	4.60	0.25	0.77	−0.19	0.83	a
116956	65515	5305.	4.45	0.07	0.97	−0.20	0.86	a
117936	66147	4791.	4.58	−0.06	0.65	−0.37	0.76	a
119332	66781	5055.	4.44	−0.14	0.90	−0.27	0.83	c
122064	68184	4635.	4.38	0.22	0.85	−0.57	0.79	c
124642	69526	4632.	4.51	−0.12	0.69	−0.56	0.74	a
128165	71181	4792.	4.56	−0.16	0.67	−0.37	0.77	a
128311	71395	4984.	4.51	0.00	0.79	−0.47	0.79	a
130215	72200	5021.	4.43	0.10	0.91	−0.26	0.84	c
130307	72312	5067.	4.54	−0.26	0.78	−0.28	0.72	a
132142	73005	5265.	4.51	−0.38	0.88	−0.20	0.79	a
135599	74702	5259.	4.57	−0.22	0.81	−0.19	0.83	a
136923	75277	5178.	4.38	0.01	1.03	−0.32	0.86	c
141272	77408	5284.	4.52	−0.19	0.88	−0.20	0.84	a
143291	78241	5315.	4.54	−0.68	0.86	−0.22	0.78	a
151541	81813	5251.	4.45	−0.22	0.96	−0.19	0.86	b
152391	82588	5413.	4.44	−0.22	1.02	−0.23	0.87	a
158633	85235	5492.	4.57	−0.63	0.88	−0.26	0.78	a

a: Based on $R-I$ colour; b: based on $b-y$ and c_1 colours; c: based on $B-V$ colour.

Table 2. Physical parameters of the NStars project and the results.

HD	$T_{\rm eff}$	log g	[Fe/H]	[Fe/H]$_{\rm I}$	[Fe/H]$_{\rm II}$	Δ[Fe/H]	[Ca/H]$_{\rm I}$	[Ca/H]$_{\rm II}$	Δ[Ca/H]
59747	5043.	4.58	−0.35	−0.11	0.00	−0.11	−0.21	−0.91	0.70
72760	5266.	4.45	−0.09	0.09	−0.02	0.11	0.07	0.03	0.04
76218	5356.	4.49	−0.12	−0.01	−0.07	0.06	−0.04	0.03	−0.07
82443	5372.	4.54	−0.18	0.08	−0.05	0.13	0.01	0.01	0.00
89813	5368.	4.51	−0.17	−0.06	−0.20	0.14	−0.17	0.00	−0.17
92786	5389.	4.64	−0.29	−0.38	−0.40	0.02	−0.33	−0.61	0.28
103095	5157.	4.76	−1.08	−1.21	−1.20	−0.01	−0.99	–	–
114783	5039.	4.49	0.00	0.04	0.10	−0.06	−0.15	0.24	−0.39
116956	5317.	4.48	−0.08	0.14	0.13	0.01	0.06	0.19	−0.13
128311	4720.	4.53	−0.57	−0.17	0.16	−0.33	−0.39	0.30	−0.69
130307	4981.	4.56	−0.41	−0.24	−0.16	−0.08	−0.33	−0.06	−0.27
141272	5299.	4.55	−0.17	0.05	0.03	0.02	−0.01	−0.16	0.15
143291	5356.	4.61	−0.36	−0.29	−0.27	−0.02	−0.22	−0.07	−0.15
152391	5290.	4.30	−0.12	0.00	0.14	−0.14	−0.06	0.06	−0.12

Table 3. The LTE abundances for the program stars.

HD	$[Fe/H]_I$	$[Fe/H]_{II}$	[O/H]	[Na/H]	[Mg/H]	[Al/H]	[Si/H]
21742	0.32	0.45	0.14	0.39	0.27	0.25	0.41
24238	−0.50	−0.48	−0.14	−0.39	−0.17	−0.27	−0.25
29883	−0.07	−0.22	−0.21	−0.01	−0.08	−0.02	−0.12
32237	−0.47	−0.64	−0.29	−0.45	−0.37	−0.38	−0.46
37008	−0.51	−0.45	−0.06	−0.40	−0.21	−0.30	−0.23
41593	0.13	0.00	−0.08	0.07	−0.09	−0.05	−0.05
51866	0.01	0.04	0.08	0.16	−0.04	−0.05	0.07
59747	−0.03	−0.08	0.06	0.01	−0.12	−0.10	−0.08
60272	−0.07	−0.19	−0.16	−0.03	−0.04	−0.13	−0.12
72760	0.16	−0.07	0.03	0.05	0.08	0.04	0.05
76218	−0.01	−0.10	−0.04	−0.05	−0.12	−0.10	−0.04
82443	−0.01	−0.05	0.11	−0.09	−0.20	−0.25	−0.09
84035	0.25	0.44	0.07	0.43	0.15	0.15	0.30
87883	0.07	0.31	0.35	−0.10	0.02	−0.07	0.21
89813	−0.02	−0.33	−0.17	0.06	−0.04	−0.05	−0.12
92786	−0.42	−0.56	−0.24	−0.32	−0.33	−0.33	−0.40
94765	0.18	0.13	−0.14	0.11	−0.08	−0.04	0.03
97658	−0.22	−0.31	−0.22	−0.19	−0.22	−0.18	−0.22
98281	−0.22	−0.26	−0.13	−0.25	−0.17	−0.19	−0.17
102195	0.15	0.06	−0.04	−0.01	0.01	0.00	0.06
103095	−1.27	−1.31	−0.55	−1.54	−1.08	−1.21	−1.12
103847	0.15	0.13	−0.09	−0.01	−0.01	−0.03	0.06
105631	0.20	0.21	0.04	0.09	0.14	0.08	0.19
108984	0.16	−0.02	−0.06	0.17	0.03	0.10	0.08
114783	0.24	0.08	−0.30	0.18	0.13	0.18	0.15
116956	0.18	0.19	0.18	0.10	0.07	−0.04	0.11
117936	0.09	0.25	0.22	0.17	−0.03	−0.09	0.07
119332	−0.07	0.01	0.14	−0.16	−0.17	−0.20	0.02
122064	0.18	0.42	0.56	0.17	0.18	0.16	0.33
124642	0.07	0.27	0.12	0.02	−0.08	−0.17	0.07
128165	−0.01	0.06	−0.03	0.03	−0.13	−0.11	0.04
128311	0.16	0.18	0.04	0.18	−0.02	−0.01	0.03
130215	0.13	0.27	0.29	−0.03	0.06	−0.06	0.19
130307	−0.12	−0.16	−0.25	−0.22	−0.19	−0.22	−0.14
132142	−0.30	−0.40	−0.18	−0.19	−0.21	−0.15	−0.28
135599	−0.02	−0.11	0.09	−0.06	−0.10	−0.16	−0.11
136923	−0.12	0.01	0.21	−0.16	−0.16	−0.21	−0.14
141272	0.07	0.04	0.08	−0.11	−0.13	−0.20	−0.09
143291	−0.33	−0.37	−0.13	−0.24	−0.31	−0.29	−0.39
151541	−0.19	−0.12	−0.01	−0.38	−0.18	−0.17	−0.13
152391	0.05	0.08	0.02	0.00	−0.06	−0.12	0.00
158633	−0.26	−0.52	−0.28	−0.21	−0.26	−0.28	−0.42

Table 3. continued.

HD	$[Ca/H]_I$	$[Ca/H]_{II}$	[Sc/H]	[Ti/H]	[V/H]	[Cr/H]	[Ni/H]	[Ba/H]	[K/H]
21742	0.08	0.36	0.60	0.16	0.23	0.36	0.33	0.08	0.30
24238	−0.38	−0.31	−0.18	−0.26	−0.37	−0.40	−0.56	−0.85	−0.25
29883	−0.13	0.00	0.09	0.23	0.25	−0.06	−0.19	−0.25	0.03
32237	−0.38	−0.29	−0.33	−0.25	−0.39	−0.47	−0.57	−0.83	−0.14
37008	−0.44	−0.16	−0.21	−0.27	−0.41	−0.49	−0.56	−0.85	−0.21
41593	0.07	−0.17	0.16	0.15	0.16	0.16	−0.05	0.05	0.24
51866	−0.12	−0.09	0.30	0.13	0.19	−0.14	−0.07	−0.23	0.11
59747	−0.07	−1.02	0.07	0.16	0.16	0.11	−0.18	−0.17	0.10
60272	−0.06	−0.26	−0.02	0.00	−0.05	0.01	−0.17	−0.22	0.06
72760	0.18	−0.06	0.25	0.23	0.20	0.30	0.03	0.15	0.21
76218	−0.03	0.02	0.12	0.01	−0.06	−0.03	−0.16	−0.03	0.16
82443	−0.08	0.07	0.06	0.03	−0.04	−0.02	−0.19	0.01	0.20
84035	0.07	0.72	0.49	0.20	0.33	0.19	0.20	−0.14	0.03
87883	−0.12	0.24	0.28	−0.07	0.01	−0.01	0.00	−0.23	−0.11
89813	−0.10	−0.11	−0.02	0.14	0.08	−0.09	−0.13	−0.39	0.23
92786	−0.38	−0.63	−0.30	−0.23	−0.35	−0.39	−0.52	−0.74	−0.17
94765	0.13	0.11	0.22	0.35	0.35	0.27	0.03	0.11	0.22
97658	−0.33	−0.38	0.05	−0.13	−0.15	−0.14	−0.30	−0.46	0.01
98281	−0.22	−0.25	−0.12	−0.09	−0.22	−0.17	−0.28	−0.49	0.06
102195	0.04	0.13	0.32	0.15	0.12	0.13	0.02	0.14	0.22
103095	−1.02	–	−0.84	−0.93	−1.16	−1.04	−1.35	−1.51	−0.64
103847	0.05	0.09	0.35	0.21	0.16	0.10	0.02	0.22	0.28
105631	0.07	0.24	0.40	0.20	0.10	0.31	0.14	0.06	0.26
108984	0.09	−0.07	0.35	0.30	0.31	0.14	0.09	−0.01	0.26
114783	0.10	0.09	0.46	0.47	0.55	0.31	0.21	0.11	0.32
116956	0.08	0.23	0.29	0.10	0.04	0.07	0.03	0.19	0.24
117936	−0.03	−0.08	0.27	0.16	0.24	0.10	−0.03	−0.13	−0.02
119332	−0.20	0.27	0.10	−0.15	−0.21	−0.17	−0.16	−0.20	−0.10
122064	−0.09	–	0.40	0.12	0.16	0.14	0.14	−0.18	−0.08
124642	−0.10	0.21	0.17	−0.03	0.09	−0.03	−0.11	−0.14	−0.19
128165	−0.19	−0.09	0.21	0.04	0.12	−0.05	−0.12	−0.28	−0.12
128311	0.04	0.14	0.26	0.31	0.40	0.22	−0.02	0.05	0.16
130215	−0.08	0.41	0.34	−0.12	−0.08	0.09	0.02	0.01	−0.01
130307	−0.19	−0.12	0.10	−0.01	−0.05	−0.16	−0.27	−0.17	−0.12
132142	−0.19	−0.15	0.00	0.00	−0.13	−0.35	−0.40	−0.56	0.00
135599	0.08	–	0.05	0.11	0.06	0.12	−0.18	−0.04	0.10
136923	−0.18	−0.08	0.08	−0.22	−0.39	−0.22	−0.21	−0.13	−0.01
141272	−0.01	−0.15	0.23	0.03	−0.02	0.10	−0.11	0.07	0.14
143291	−0.27	−0.09	−0.11	−0.13	−0.38	−0.28	−0.45	−0.54	0.06
151541	−0.21	−0.25	0.02	−0.23	−0.27	−0.23	−0.24	−0.36	−0.20
152391	−0.02	−0.03	0.14	0.05	−0.07	0.09	−0.10	0.10	0.20
158633	−0.19	–	−0.34	−0.03	−0.13	−0.21	−0.36	−0.51	0.08

Table 4. Atomic line data.

λ [Å]	χl [eV]	$\log(gf)$	$\sigma\Gamma_6$
O I $\log(\epsilon_\odot) = 8.83$			
6158.18	10.74	−0.290	2.5
7771.954	9.14	0.333	2.5
7774.177	9.14	0.188	2.5
7775.395	9.14	−0.034	2.5
Na I $\log(\epsilon_\odot) = 6.33$			
5889.973	0.00	0.112	2.0
5895.940	0.00	−0.191	2.0
6154.230	2.10	−1.570	2.0
6160.753	2.10	−1.270	2.0
8194.836	2.10	0.490	2.0
Mg I $\log(\epsilon_\odot) = 7.58$			
7657.606	5.11	−1.186	2.5
8712.701	5.93	−1.260	2.5
8717.833	5.93	−0.970	2.5
Al I $\log(\epsilon_\odot) = 6.47$			
6696.020	3.14	−1.342	2.5
6698.670	3.14	−1.873	2.5
7835.317	4.02	−0.580	2.5
7836.130	4.02	−0.400	2.5
Si I $\log(\epsilon_\odot) = 7.55$			
5797.865	4.95	−2.050	1.3
5948.548	5.08	−1.190	1.5
6125.026	5.61	−1.495	1.3
6142.494	5.62	−1.434	1.3
6145.020	5.62	−1.422	1.3
6721.844	5.86	−1.060	1.3
7034.910	5.87	−0.810	1.5
7405.790	5.61	−0.681	1.5
7800.000	6.18	−0.668	1.3
7918.383	5.95	−0.536	1.5
7932.351	5.96	−0.352	1.5
8728.024	6.18	−0.475	1.3
8742.466	5.87	−0.571	1.3
Ca I $\log(\epsilon_\odot) = 6.36$			
5857.459	2.93	0.112	1.8
5867.572	2.93	−1.610	1.8
6102.727	1.88	−0.819	2.3
6161.295	2.52	−1.192	1.8
6163.754	2.52	−1.286	2.0
6166.440	2.52	−1.189	1.8
6169.044	2.52	−0.797	1.8
6169.564	2.52	−0.511	2.0
6439.083	2.52	0.164	1.5
6449.820	2.52	−0.502	1.5
6455.605	2.52	−1.350	1.5
6493.788	2.52	−0.092	0.8
6499.654	2.52	−0.818	1.8
6717.687	2.71	−0.524	1.8
6471.668	2.52	−0.694	1.8
Ca II $\log(\epsilon_\odot) = 6.36$			
8248.802	7.51	0.572	1.8
Sc II $\log(\epsilon_\odot) = 3.10$			
6604.600	1.36	−1.300	2.5
Ti I $\log(\epsilon_\odot) = 5.02$			
5866.461	1.07	−0.805	1.5
5953.170	1.89	−0.329	1.5
6126.224	1.07	−1.320	1.5
6258.110	1.44	−0.431	1.5

Table 4. continued.

λ [Å]	χl [eV]	$\log(gf)$	$\sigma\Gamma_6$
Ti I $\log(\epsilon_\odot) = 5.02$			
6261.106	1.43	−0.479	1.5
8426.514	0.83	−1.253	1.5
8435.655	0.84	−1.023	1.5
V I $\log(\epsilon_\odot) = 4.00$			
6090.216	1.08	−0.139	1.5
6216.358	0.28	−0.845	1.5
Cr I $\log(\epsilon_\odot) = 5.67$			
7355.891	2.89	−0.285	2.5
7400.188	2.90	−0.166	2.5
6979.806	3.46	−0.314	2.5
Ni I $\log(\epsilon_\odot) = 6.25$			
5805.226	4.17	−0.587	2.5
6086.288	4.26	−0.530	2.5
6108.125	1.68	−2.675	2.5
6111.078	4.09	−0.870	2.5
6128.984	1.68	−3.413	2.5
6130.141	4.26	−0.960	2.5
6176.816	4.09	−0.260	2.5
6327.604	1.68	−3.110	2.5
6482.809	1.93	−2.739	2.5
6586.319	1.95	−2.733	2.5
6643.638	1.68	−2.154	2.5
6767.784	1.83	−2.173	2.5
6772.321	3.66	−0.980	2.5
7110.905	1.93	−2.980	2.5
7122.206	3.54	−0.229	2.5
7385.244	2.74	−2.051	2.5
7414.514	1.99	−2.570	2.5
7422.286	3.63	−0.325	2.5
7525.118	3.63	−0.653	2.5
7574.048	3.83	−0.607	2.5
7714.310	1.93	−1.193	2.5
7715.591	3.70	−0.954	2.5
7727.616	3.68	−0.161	2.5
7748.894	3.70	−0.328	2.5
7788.933	1.95	−2.075	2.5
7797.588	3.90	−0.325	2.5
Ba II $\log(\epsilon_\odot) = 2.22$			
5853.688	0.60	−0.910	3.0
6141.727	0.70	−0.077	3.0
6496.908	0.60	−0.377	3.0
K I $\log(\epsilon_\odot) = 5.10$			
7698.977	0.00	−0.168	1.5
Fe II $\log(\epsilon_\odot) = 7.51$			
5991.378	3.15	−3.557	2.5
6149.249	3.89	−2.837	2.5
6247.562	3.89	−2.431	2.5
6416.928	3.89	−2.520	2.5
6432.683	2.89	−3.501	2.5
6516.083	2.89	−3.199	2.5
6456.391	3.90	−2.182	2.5
7711.731	3.90	−2.453	2.5
Fe I $\log(\epsilon_\odot) = 7.51$			
5806.732	4.61	−0.881	1.4
5809.224	3.88	−1.726	1.4
5852.228	4.55	−1.101	1.4
5856.096	4.29	−1.547	1.4
5905.680	4.65	−0.732	1.4

Table 4. continued.

λ [Å]	χl [eV]	$\log(gf)$	$\sigma\Gamma_6$
Fe I $\log(\epsilon_\odot) = 7.51$			
5916.257	2.45	−2.944	1.3
5927.797	4.65	−1.101	1.4
5929.682	4.55	−1.195	1.4
5934.665	3.93	−1.152	1.4
5952.726	3.98	−1.429	1.4
5956.706	0.86	−4.498	1.1
6027.059	4.07	−1.089	1.4
6065.494	2.61	−1.572	1.4
6079.016	4.65	−1.005	1.4
6093.649	4.61	−1.285	1.4
6096.671	3.98	−1.770	1.4
6137.002	2.20	−2.865	1.2
6137.702	2.59	−1.370	1.4
6151.623	2.18	−3.282	1.2
6136.624	2.45	−1.405	1.3
6157.733	4.07	−1.220	1.4
6165.363	4.14	−1.473	1.4
6173.341	2.22	−2.880	1.2
6187.995	3.94	−1.728	1.4
6200.321	2.61	−2.442	1.4
6219.287	2.20	−2.430	1.2
6252.565	2.40	−1.727	1.3
6265.141	2.18	−2.550	1.2
6297.799	2.22	−2.733	1.2
6322.694	2.59	−2.446	1.4
6330.852	4.73	−1.158	1.4
6344.155	2.43	−2.897	1.3
6358.687	0.86	−4.166	1.1
6380.750	4.19	−1.290	1.4
6419.956	4.73	−0.195	1.4
6430.856	2.18	−1.976	1.2
6481.878	2.28	−2.972	1.2
6494.994	2.40	−1.239	1.3
6496.472	4.79	−0.537	1.4
6498.945	0.96	−4.699	1.1
6593.884	2.43	−2.422	1.3
6609.118	2.56	−2.661	1.4
6750.164	2.42	−2.604	1.3
6752.716	4.64	−1.280	1.4
6810.267	4.61	−0.986	1.4
6828.596	4.64	−0.842	1.4
6841.341	4.61	−0.630	1.4
6842.689	4.64	−1.078	1.4
6843.655	4.55	−0.847	1.4
6858.155	4.61	−0.930	1.4
6945.210	2.42	−2.452	1.3
6978.862	2.48	−2.490	1.3
6999.885	4.10	−1.350	1.4
7022.957	4.19	−1.185	1.4
7038.220	4.22	−1.156	1.4
7090.390	4.23	−1.092	1.4
7130.925	4.22	−0.748	1.4
7132.985	4.07	−1.628	1.4
7723.210	2.28	−3.617	1.2
7912.870	0.86	−4.848	1.1
8327.061	2.20	−1.440	1.2
8611.812	2.84	−1.919	1.4
8674.756	2.83	−1.730	1.4
8688.642	2.18	−1.202	1.2
8757.199	2.84	−2.026	1.4

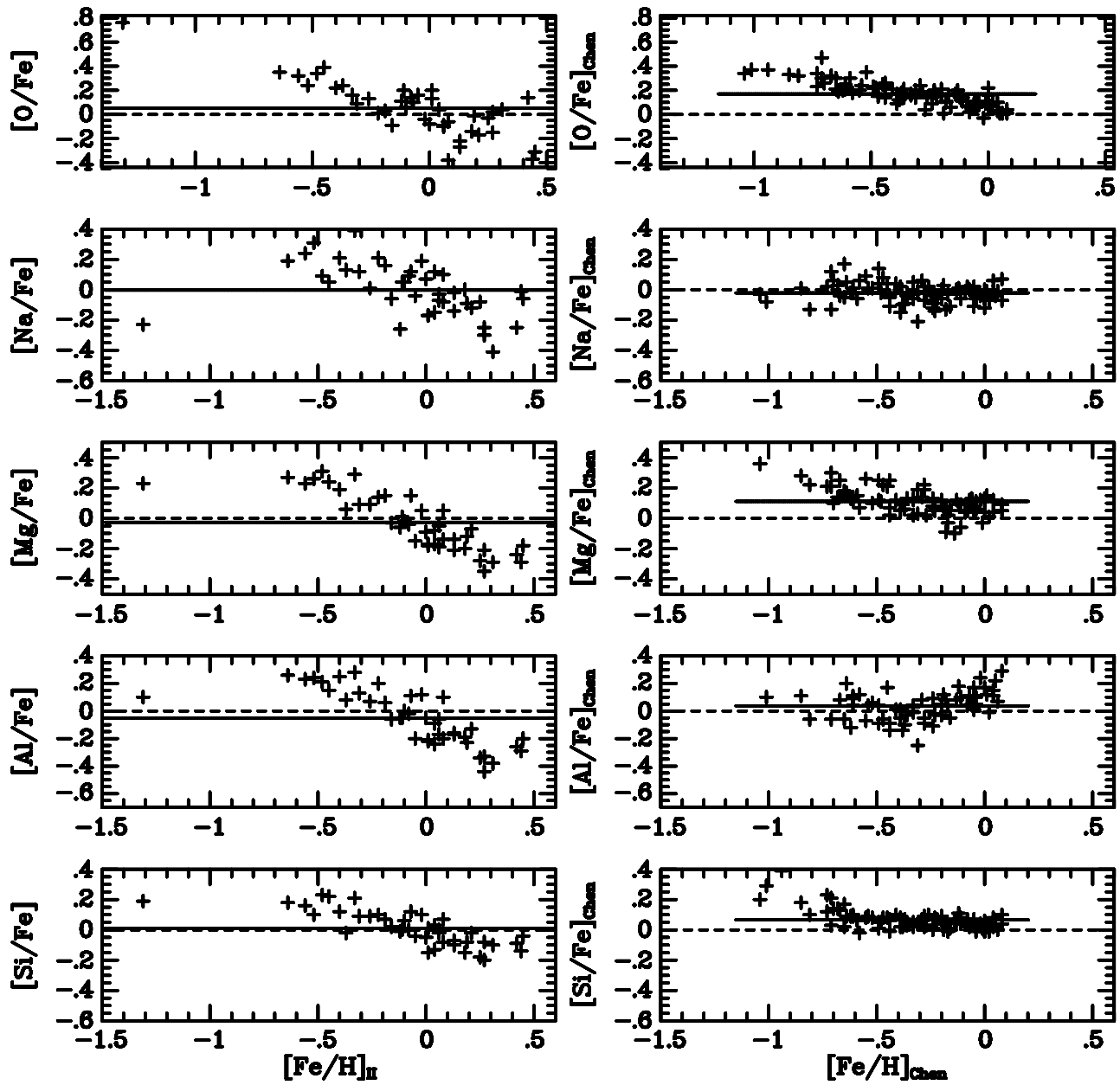

Fig. 12. The comparison of general trends of oxygen, sodium, magnesium, aluminium and silicon.

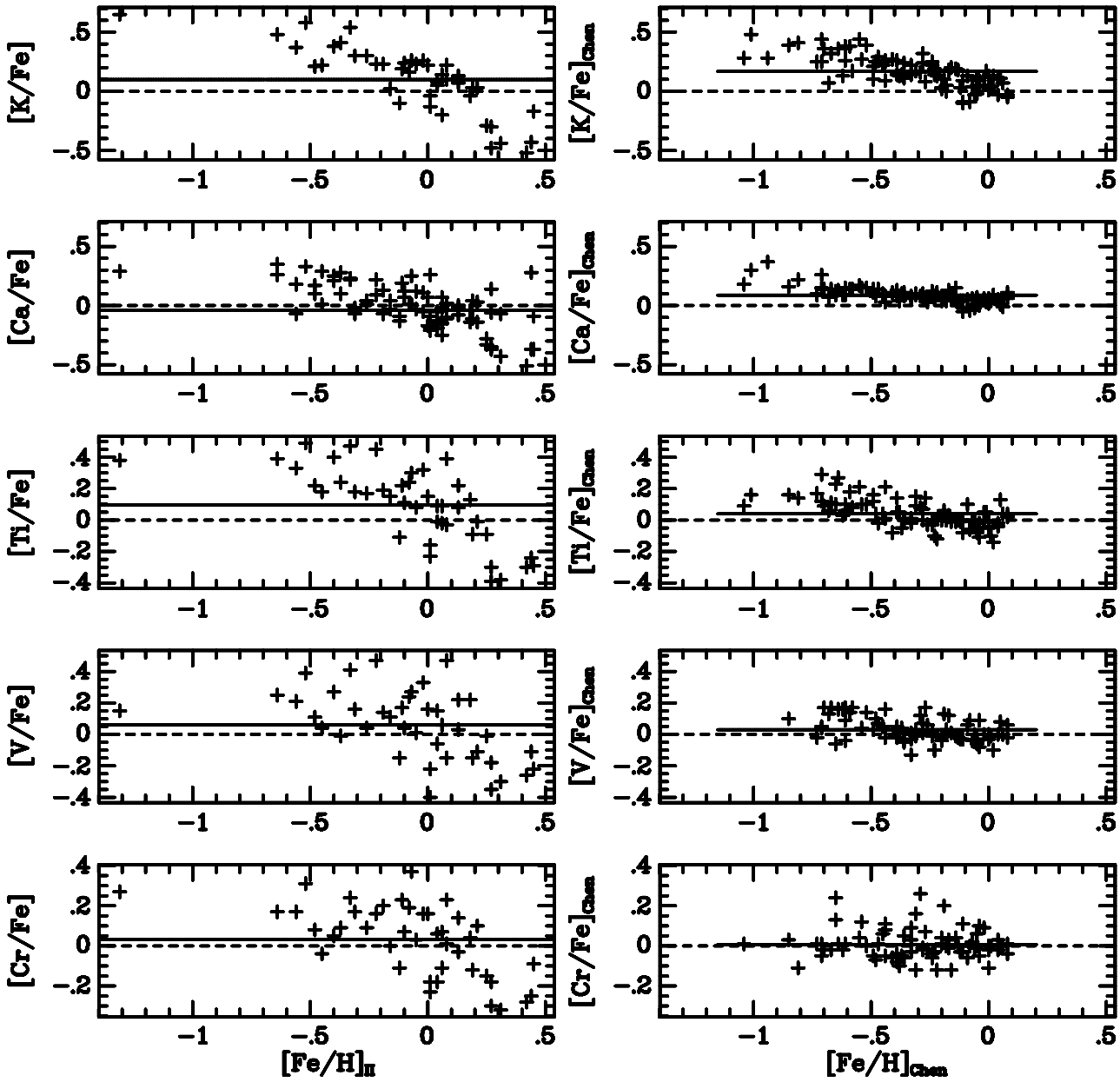

Fig. 13. Comparisons of general trends of potassium, calcium (both $[Ca/Fe]_I$ and $[Ca/Fe]_{II}$), titanium, vanadium and chromium.

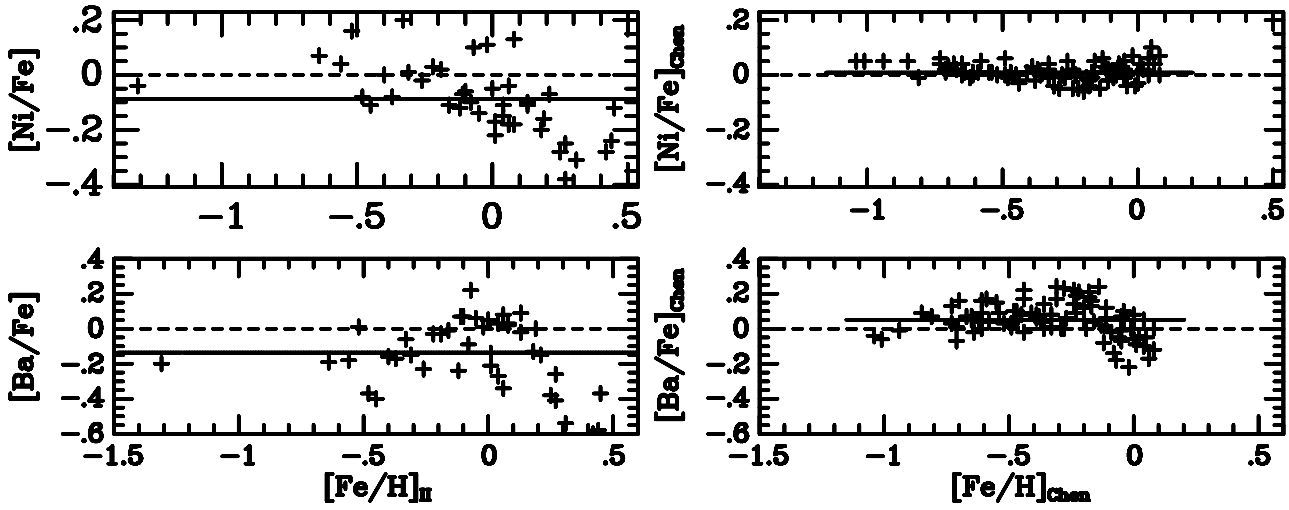

Fig. 14. Comparisons of general trends of nickel and barium.